Edge-preserving smoothing for segmentation of seismic images

Adam Halpert

ABSTRACT

In many disciplines, pre-processing images by smoothing is common prior to automatic image segmentation; however, traditional smoothing blurs boundaries and can be counterproductive, especially for seismic images. Here, an edge-preserving smoothing technique based on directional maximum homogeneity is introduced for 3D seismic images, and tested on both synthetic and field data. Edge-preserving smoothing is shown to both decrease the level of noise in an image, and improve the accuracy of automatic segmentation results. In addition, a "hybrid" smoothing technique blending traditional and edge-preserving smoothing combines the advantages of each and produces encouraging results.

INTRODUCTION

Because it can reduce the time and effort required for human-intensive image interpretation tasks, automatic image segmentation is a tool employed in a variety of disciplines – for example, medical imaging, photo editing/image processing, and seismic imaging and interpretation. A particular area of interest involves the pre-processing of images prior to automatic segmentation (Zahedi and Thomas, 1993). Here, I investigate the usefulness of an edge-preserving smoothing (EPS) technique for segmentation of seismic images.

A primary use for automatic seismic image segmentation is for identification and location of complex subsurface salt bodies, a task that is extremely time-consuming when undertaken manaully. In the examples here, the pairwise region comparison (PRC) segmentation algorithm (Felzenszwalb and Huttenlocher, 2004) is employed because it is designed to operate extremely efficiently, even when extended to three dimensions and adapted for seismic data (Halpert et al., 2010). However, like any segmentation algorithm, its accuracy can suffer, especially where boundaries are discontinuous or chaotic (for example, see Figure 10(a)). In such cases, smoothing the image before the segmentation procedure can reduce unwanted noise and improve performance of many image processing algorithms (Zahedi and Thomas, 1993).

For seismic images, naive box or Gaussian smoothing has clear disadvantages. When segmenting seismic images, clear and sharp boundaries are preferable for an accurate result; simple smoothing tends to blur these boundaries, or even render

them uninterpretable if two reflectors are very close together (see Figure 3(a)). A variety of "smarter" smoothing or noise-reduction approaches for seismic data have been proposed, including inversion-based techniques like PEFs (Claerbout, 2005; Guitton, 2005), structure or dip-oriented filtering (Fehmers and Hocker, 2003), or bilateral filtering (Hale, 2011). Unfortunately, these algorithms require computationally-intensive inversions and/or solutions to differential equations like the diffusion equation, or prior information in the form of dip or structure interpretations. Therefore, a cheap, efficient smoothing algorithm that preserves sharp boundaries would represent a useful pre-processing step for seismic image segmentation.

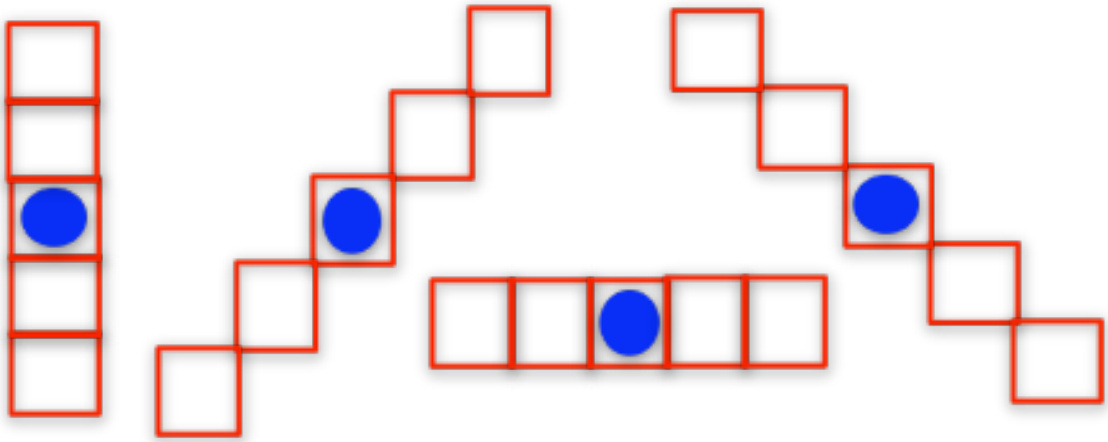

Figure 1: A set of 1D bar masks used to determine the most homogeneous orientation around a central pixel on a 2D image. For 3D images, additional masks would extend out of the page. [**NR**]

EPS TECHNIQUE

Edge-preserving smoothing is a common goal in many image processing disciplines. An early form of EPS was median smoothing (Tukey, 1971), in which a central pixel is assigned the median pixel value from a neighborhood around it. Later, a method aiming for increased directional accuracy in EPS was proposed by Tomita and Tsuji (1977), in which the average value of the most homogeneous of several neighborhoods extending from the pixel was calculated. More recently, Zahedi and Thomas (1993) introduced the concept of "bar masks," one-dimensional vectors of pixels that extend in different directions from the central pixel (Figure 1). This approach further increases directional discrimination in "maximum homogeneity" filtering approaches. Furthermore, Zahedi and Thomas (1993) assigned the median of the most homogeneous bar mask to the central pixel, rather than the average value; this improved the preservation of sharp edges in an image, and makes it attractive for use in seismic images.

A very similar approach has already been proposed for use on three-dimensional

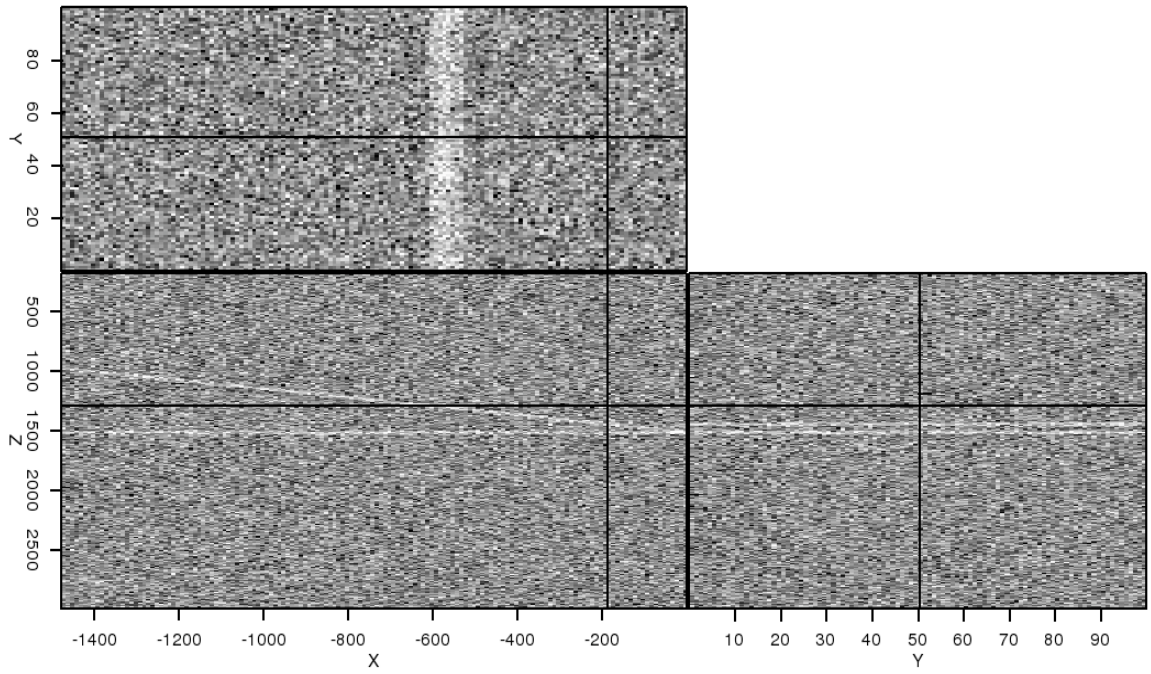

Figure 2: A simple 2.5-D synthetic consisting of two planar reflectors and contaminated with random noise. The high level of noise makes it difficult to distinguish the two reflectors at the indicated location. [**ER**]

seismic images. AlBinHassan et al. (2006) constructed many 3D neighborhoods around a central pixel, and used the average value of the most homogeneous block. For this method and that of Zahedi and Thomas (1993), maximum homogeneity is determined by calculating the variance of the individual bar masks or 3D blocks:

$$\sigma = \left[\frac{1}{n} \sum_{i=1}^{n} (d_i - \overline{d})^2 \right]^{1/2}, \tag{1}$$

where n is the number of pixels in the bar mask or block d, and $\overline{d}$ is the average value of those pixels. The mask or block with the smallest variance has the greatest homogeneity.

The method presented here differs from this approach by incorporating two ideas from Zahedi and Thomas (1993). First, nine 1D bar masks, extending from a central pixel along each axis and diagonal of a cube enclosing the pixel, are used instead of the 3D blocks. This greatly simplifies the computational complexity of the algorithm, while at the same time preserving sharp boundaries with arbitrary orientations. Second, the median value of the bar mask with maximum homogeneity is used, rather than the average value. Again, this enhances the edge-preserving characteristics of the filter.

Synthetic example

The effectiveness of this method is best demonstrated through examples, and comparison to the traditional smoothing approach. Figure 2 is a noisy 2.5D synthetic featuring a dipping reflector pinching out onto a flat reflector. Because of the noise, it is difficult to differentiate the two reflectors near their intersection.

Ideally, smoothing the noisy image would clean up the image, and allow an interpreter to clearly see where the reflectors intersect. However, a traditional 5x5x5 box filter fails to produce this result (Figure 3(a)). While much of the noise is indeed removed, the filter has blurred the reflectors, making it impossible to distinguish between them. Furthermore, taking the difference between the noisy image and the filtered image gives an unwanted result (Figure 4(a)); it is obvious that a significant amount of coherent signal has been removed. In contrast, the maximum homogeneity (MH) filter with a mask length of 5 pixels performs better (Figure 3(b)). Not only are the two reflectors able to be distinguished much more easily in the filtered result (Figure 3(b)), but the difference calculation (Figure 4(b)) shows much less coherent signal being removed. Despite these advantages, though, more noise does remain in the MH-filtered image.

A HYBRID APPROACH

From the examples in Figure 3, it appears that traditional smoothing does perform very well in areas devoid of sharp boundaries or edges. Therefore, we can develop an approach that combines the characteristics of box smoothing in areas without edges, and takes advantage of the edge-preserving features of MH filtering when edges are present. For the MH algorithm, we already calculate variances for each of the bar masks passing through a given pixel. Comparing the largest and smallest of these calculated variances indicates the likelihood that an edge is present. If the ratio between the smallest and largest variances is large (close to 1), the pixel is in a relatively "isotropic" area, and an edge is unlikely to be present. Conversely, a smaller ratio implies that an edge is present in at least one of the bar mask orientations. If α is a user-determined threshold value, then if $\frac{\min(\sigma)}{\max(\sigma)} > \alpha$, traditional smoothing can safely be used in lieu of MH filtering for that particular location.

Figure 5 demonstrates this strategy on the synthetic example shown earlier. As the threshold value α decreases, the algorithm is more biased toward traditional smoothing; consequently, the amount of "speckle" noise decreases. However, near the two reflectors, MH filtering still holds sway. The final result is an image with the speckle noise removed as well as in the traditional smoothing result in Figure 3(a), but with the reflector edges preserved as well as the standard MH result in Figure 3(b).

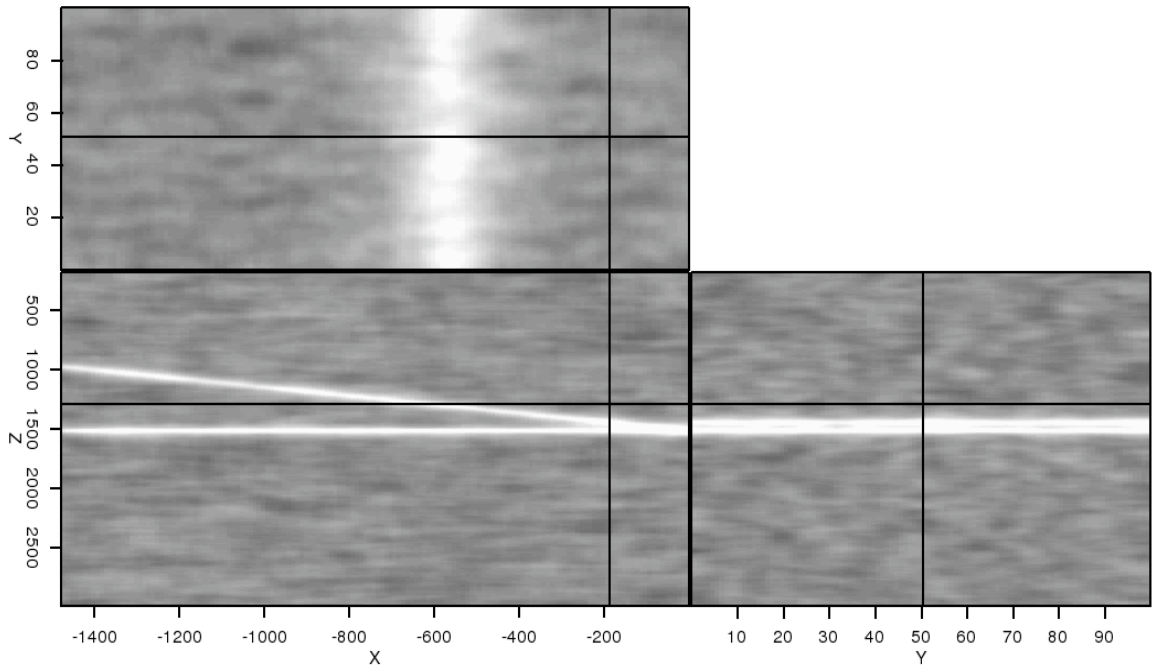

(a)

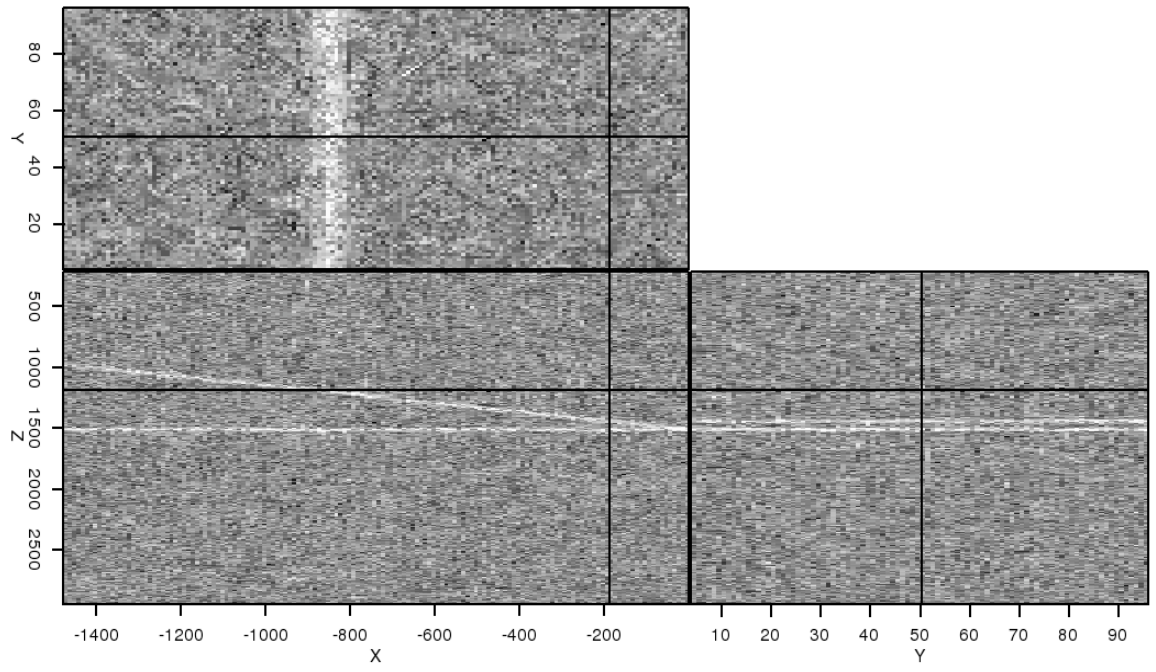

(b)

Figure 3: Results of smoothing the image in Figure 2 with (a) traditional box smoothing, and (b) maximum homogeneity (MH) filtering of the same operator length. [**ER**]

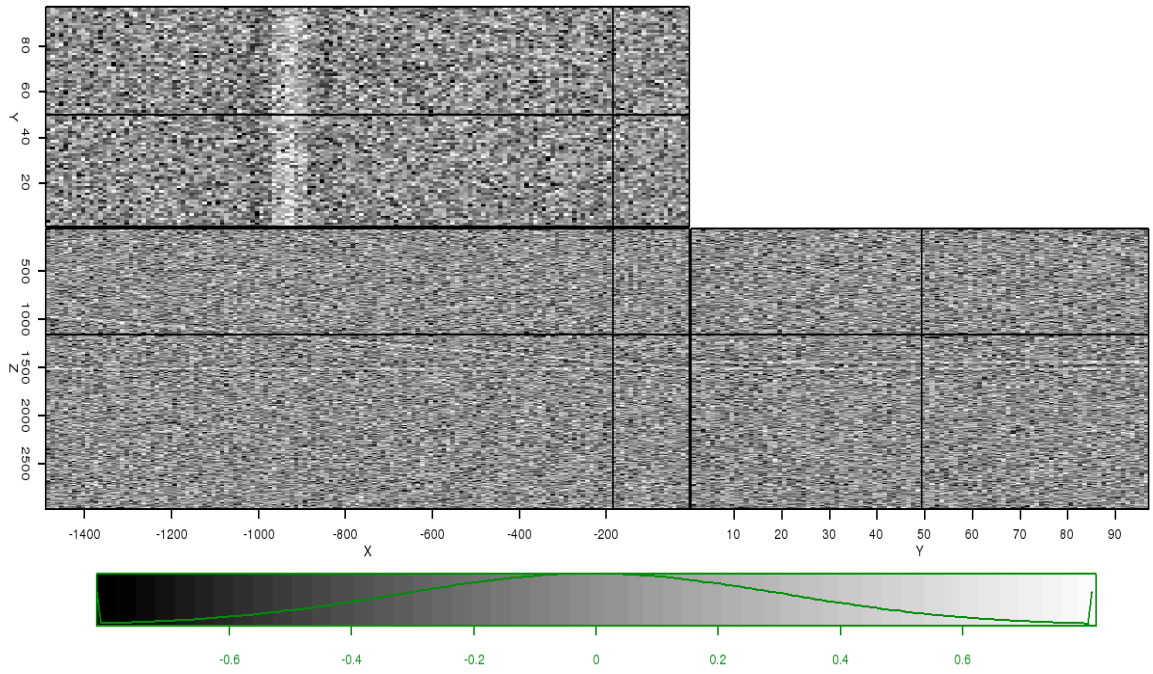

(a)

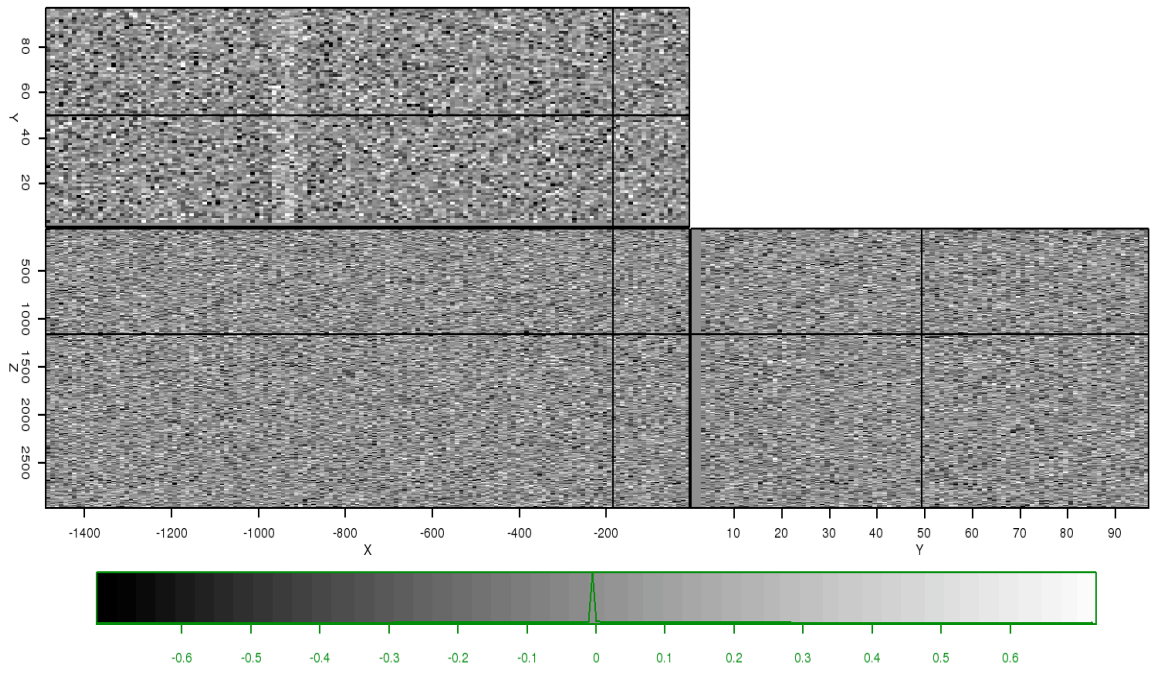

(b)

Figure 4: Results of differencing the images in Figures 2 and 3. The filtered information when using the MH filter (b) contains much less coherent signal than when using traditional smoothing (a). [**ER**]

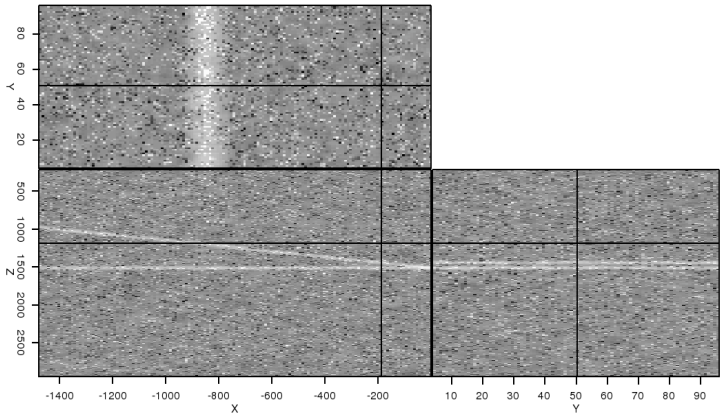

(a)

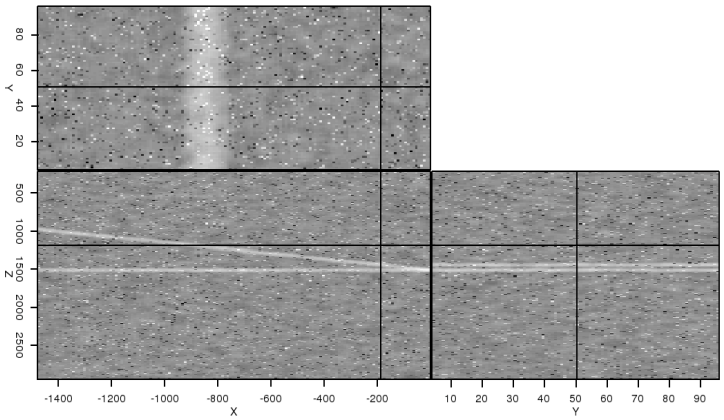

(b)

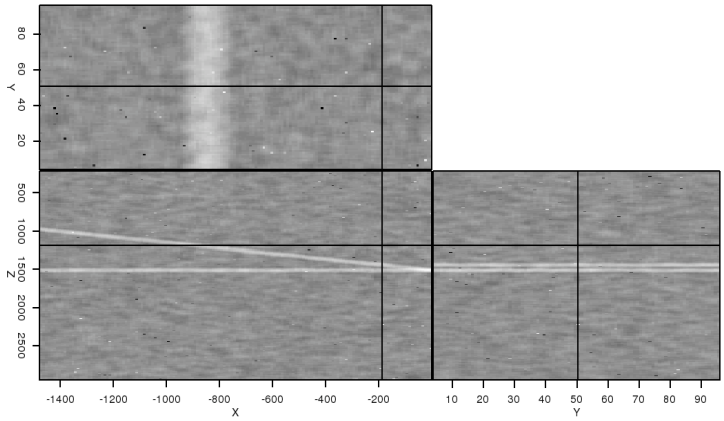

(c)

Figure 5: The results of applying the hybrid-MH filter with α set at (a) 0.5, (b) 0.25, and (c) 0.1 to the original noisy synthetic image in Figure 2. As α decreases, more speckle-noise is removed from the image, while the sharpness of the reflectors is preserved. [**ER**]

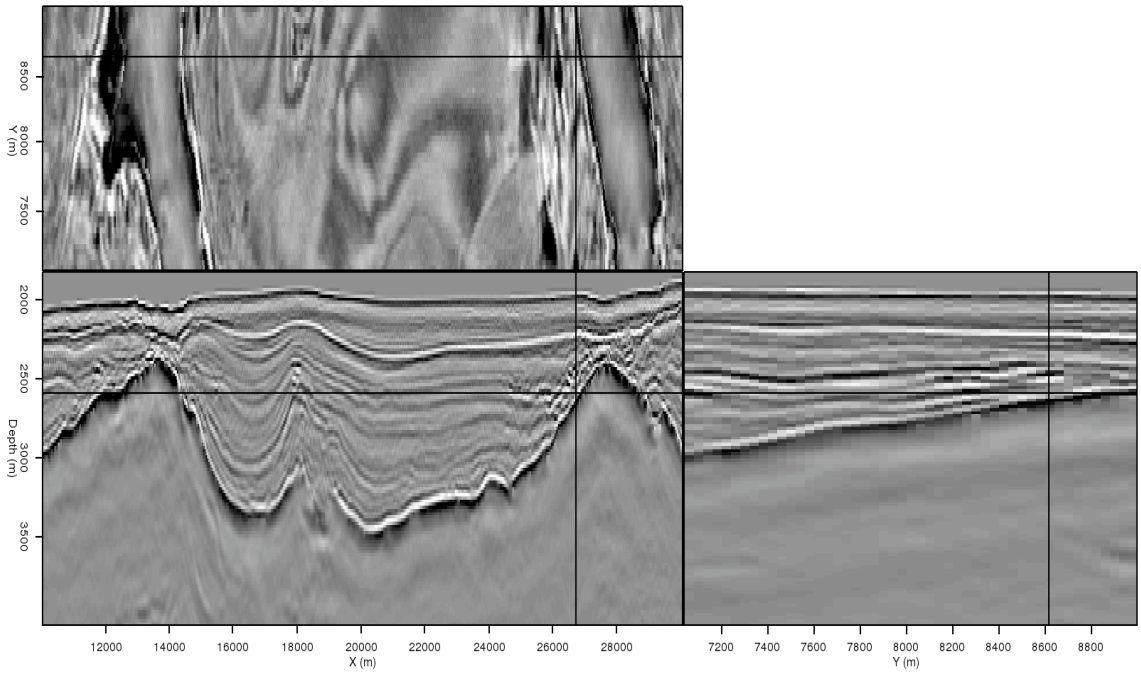

Figure 6: A 3D image from the Gulf of Mexico with a prominent but discontinuous salt boundary. [**ER**]

FIELD DATA EXAMPLES

Figure 6 shows a 3D field data image from the Gulf of Mexico. The salt boundary is clearly visible, but its discontinuous nature can pose problems for many automatic picking algorithms. Figure 7 shows the result of smoothing the image with traditional filtering (a), and the hybrid-MH method (b). The hybrid-MH filter attenuates a noticeable amount of background noise, while preserving the salt boundaries much more clearly than traditional smoothing. The difference calculations shown in Figure 8 confirm that MH-filtering removes much less coherent signal than traditional smoothing.

Figure 9 shows the effects of varying the hybrid threshold parameter α for the field data example. As α decreases, the image becomes noticeably smoother, even though the reflector boundaries remain clear. In this example, though, it is evident that the reflectors' amplitudes are being modified, which is an important consideration.

IMAGE SEGMENTATIONS

Finally, we should examine the effect of MH filtering on automatic segmentation results. Figure 10(a) is the result of segmenting the original, unfiltered image in Figure 6. "Leakages" are apparent from the salt body into the surrounding sediments, especially near the intersecting location indicators. When the MH-filtered image is

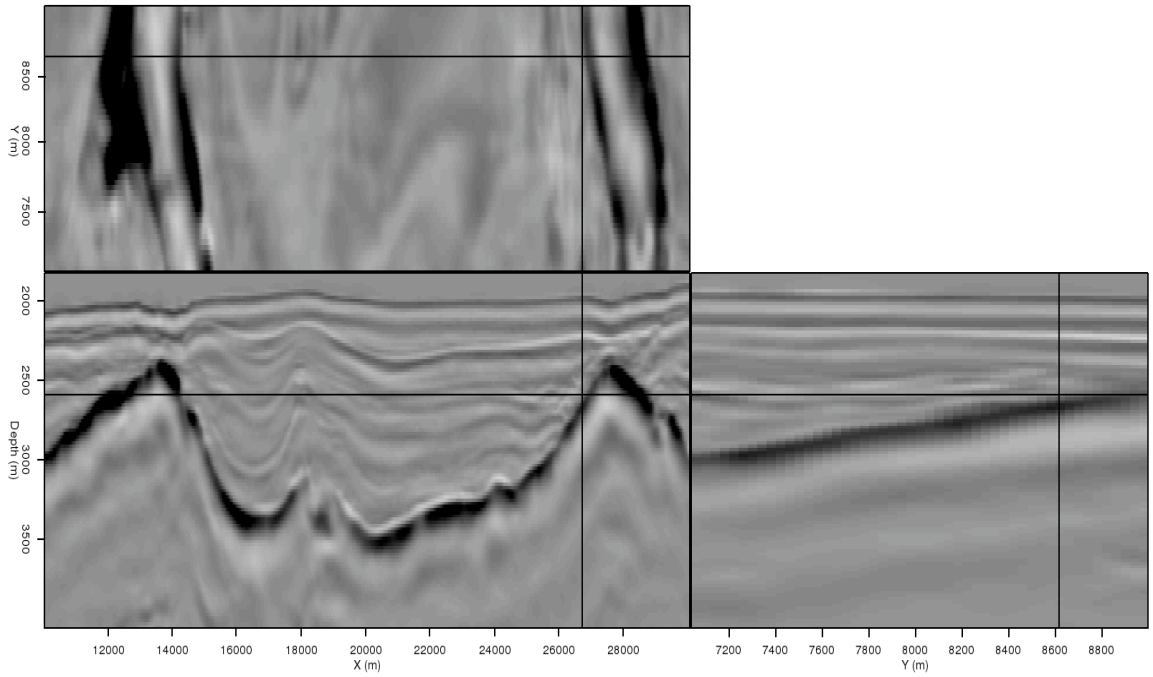

(a)

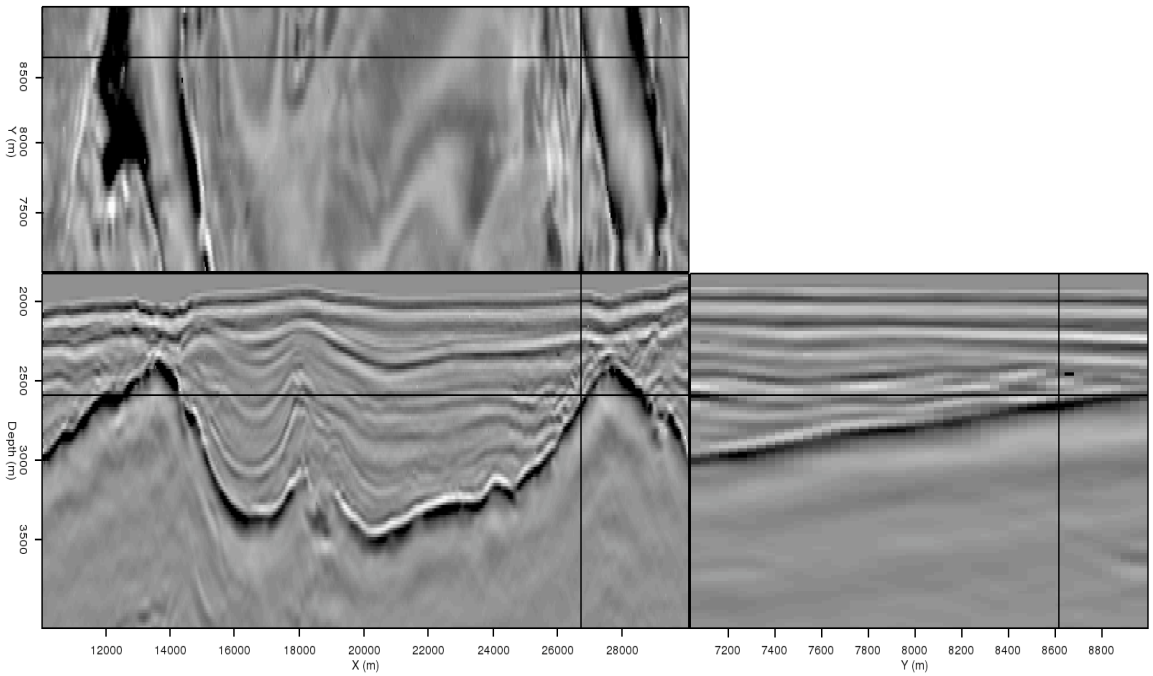

(b)

Figure 7: The image in Figure 6, smoothed with (a) a traditional box filter, and (b) a hybrid-MH filter of the same length. [**ER**]

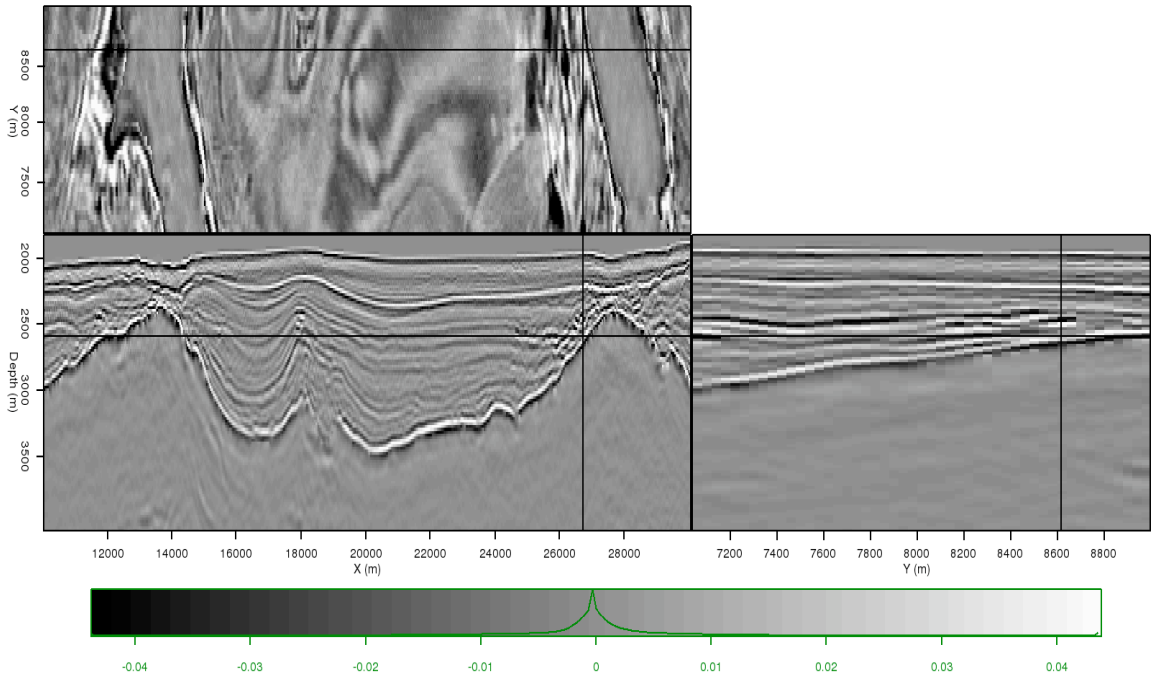

(a)

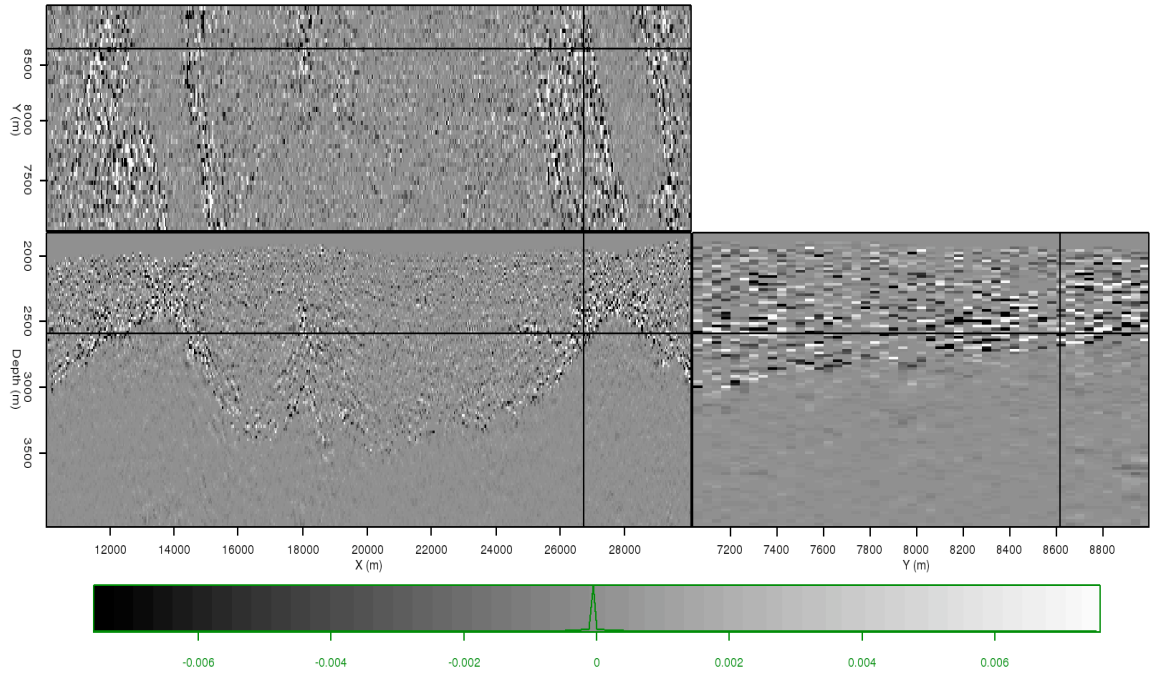

(b)

Figure 8: Results of differencing the original image in Figure 6 with (a) the image smoothed with a traditional box filter, and (b) the image smoothed with the MH filter. Again, the result in (b) shows that much less coherent signal has been removed from the image. [**ER**]

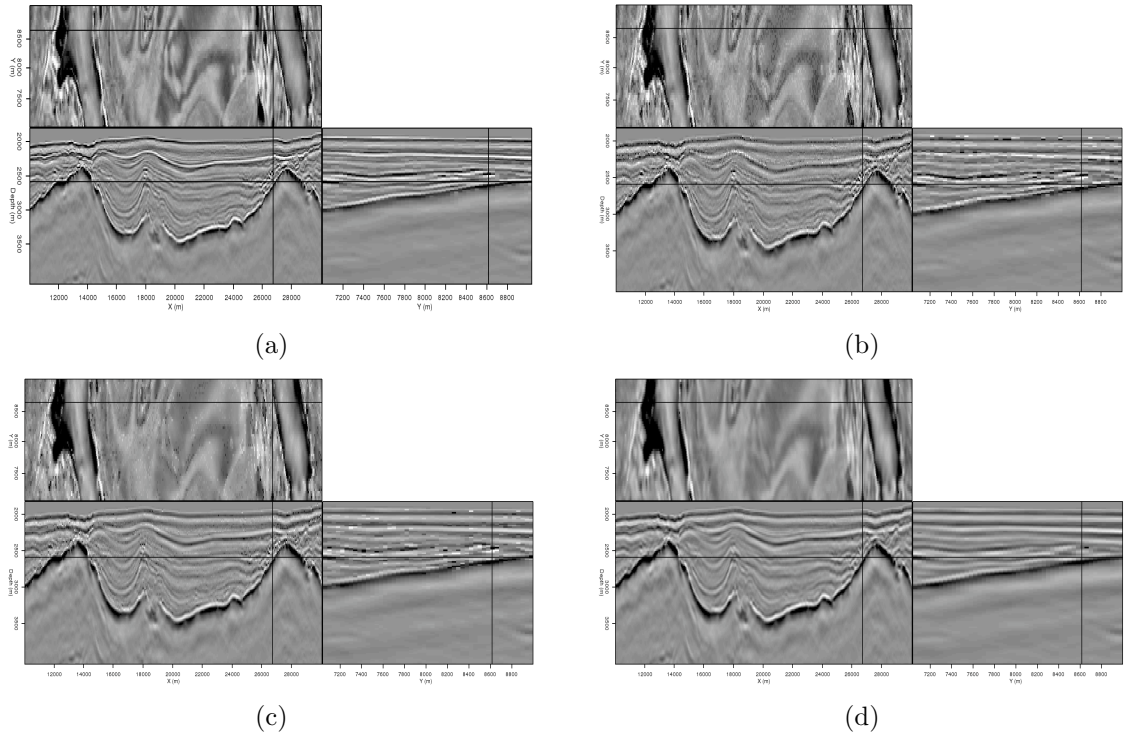

(a) (b)

(c) (d)

Figure 9: Results of applying the hybrid-MH filter on the image in Figure 6, with α set at (a) 0.5, (b) 0.2, and (c) 0.1 and (d) 0.01. While the reflector ampliltudes are affected, a great deal of speckle noise is removed at low α values. [**ER**]

segmented, however, these problems are greatly ameliorated (Figure 10(b)). A second field data example is the attempt to segment the small salt inclusion indicated in Figure 11. While segmenting the original image leads to the poor result in Figure 12(a), segmenting an MH-filtered image provides a much improved result (Figure 12(b)). In these examples, hybrid-MH filtering has allowed for more accurate segmentation results; furthermore, the computational efficiency (and simple parallelization) of the algorithm make it especially attractive since smoothing the image in these examples required only a fraction of the time needed for the already-efficient PRC segmentation algorithm.

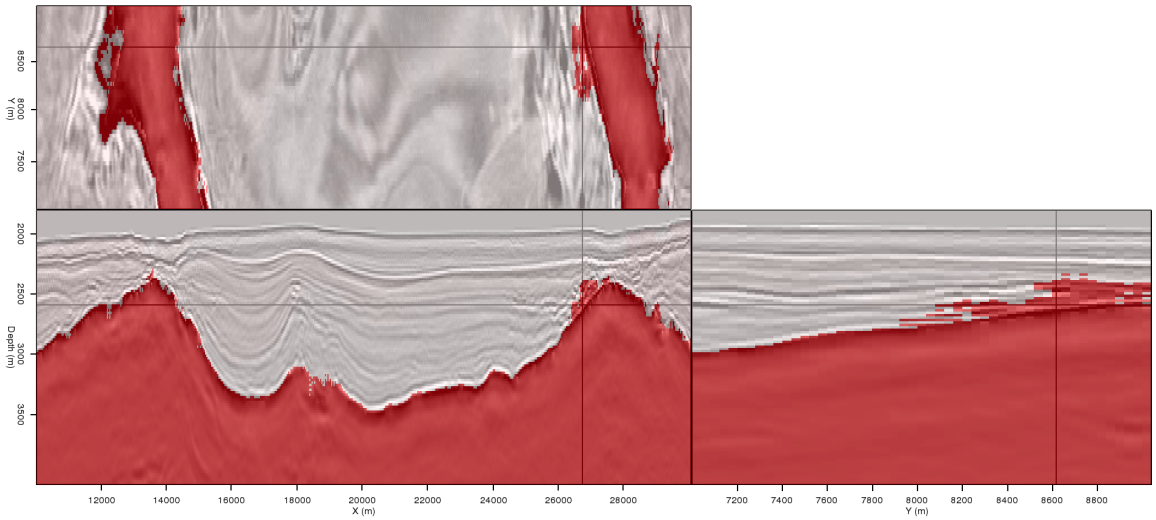

(a)

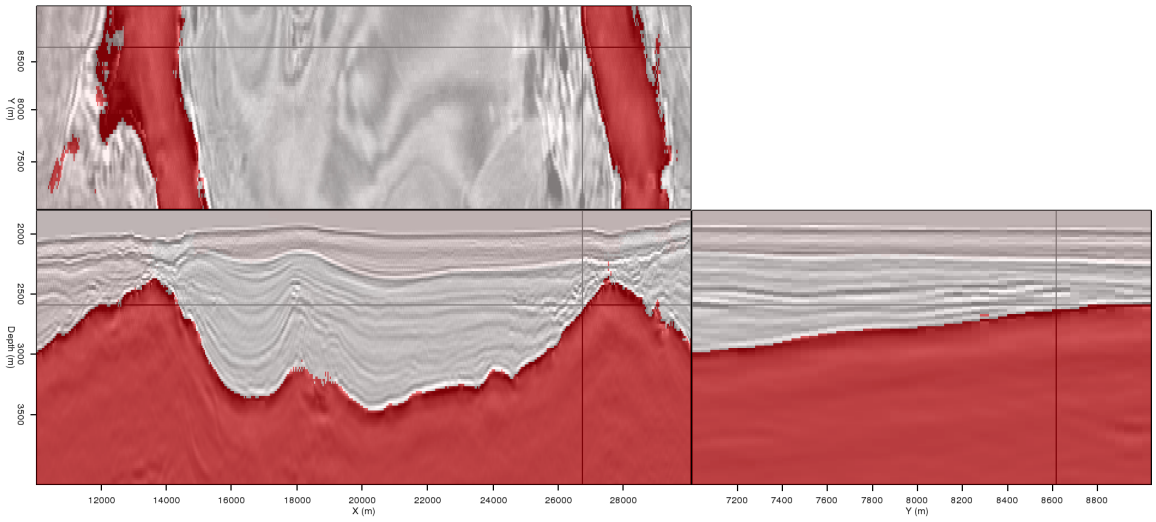

(b)

Figure 10: Automatic image segmentation results when using (a) the original, unfiltered image in Figure 6, and the MH-smoothed image in Figure 9(d). [**ER**]

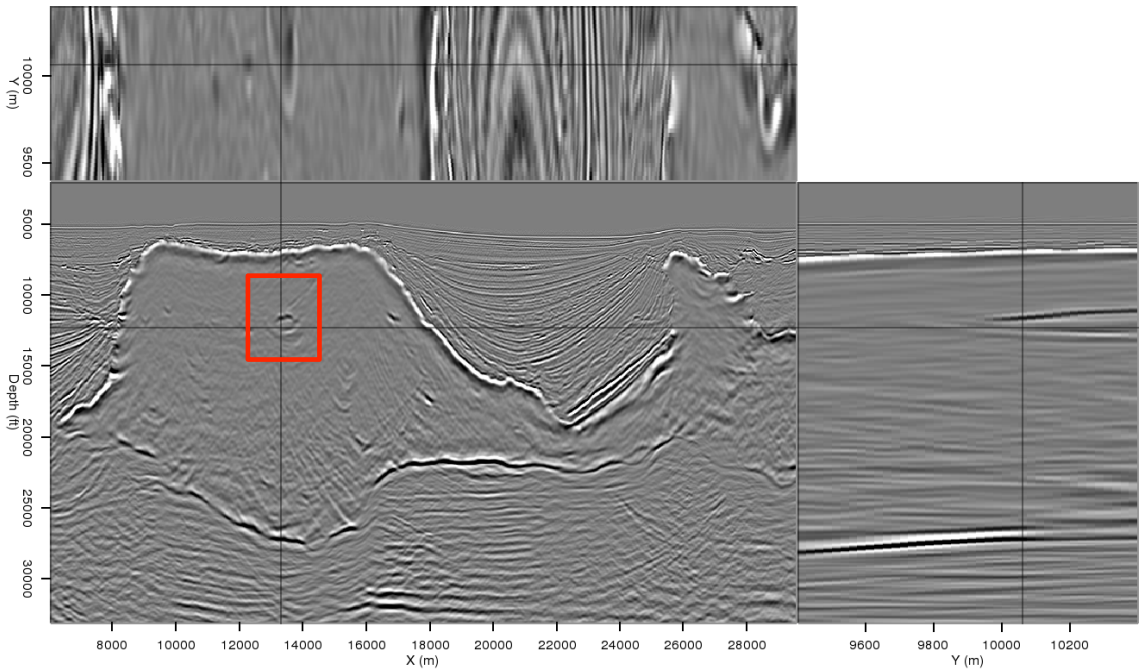

Figure 11: Another image from the Gulf of Mexico featuring an inclusion within the salt body. Further examples will be shown from the indicated area. [**ER**]

CONCLUSIONS

Automated seismic image segmentation schemes can benefit from preprocessing such as smoothing prior to segmentation. An edge-preserving smoothing method based on directional maximum homogeneity can de-noise and clean up an image, while preserving important edges such as salt boundaries. Applying the MH filtering algorithm to 3D field seismic data improves segmentation results by reducing "leakages" through boundaries. In addition, a hybrid approach combining the best aspects of traditional smoothing and MH filtering can improve noise removal while still preserving edges well.

ACKNOWLEDGMENTS

I thank WesternGeco and Unocal (Chevron) for providing the field data used for examples.

REFERENCES

AlBinHassan, N., Y. Luo, and M. N. Al-Faraj, 2006, 3D edge-preserving smoothing and applications: Geophysics, **71**, P5–P11.

Claerbout, J., 2005, Image estimation by example: Stanford University.

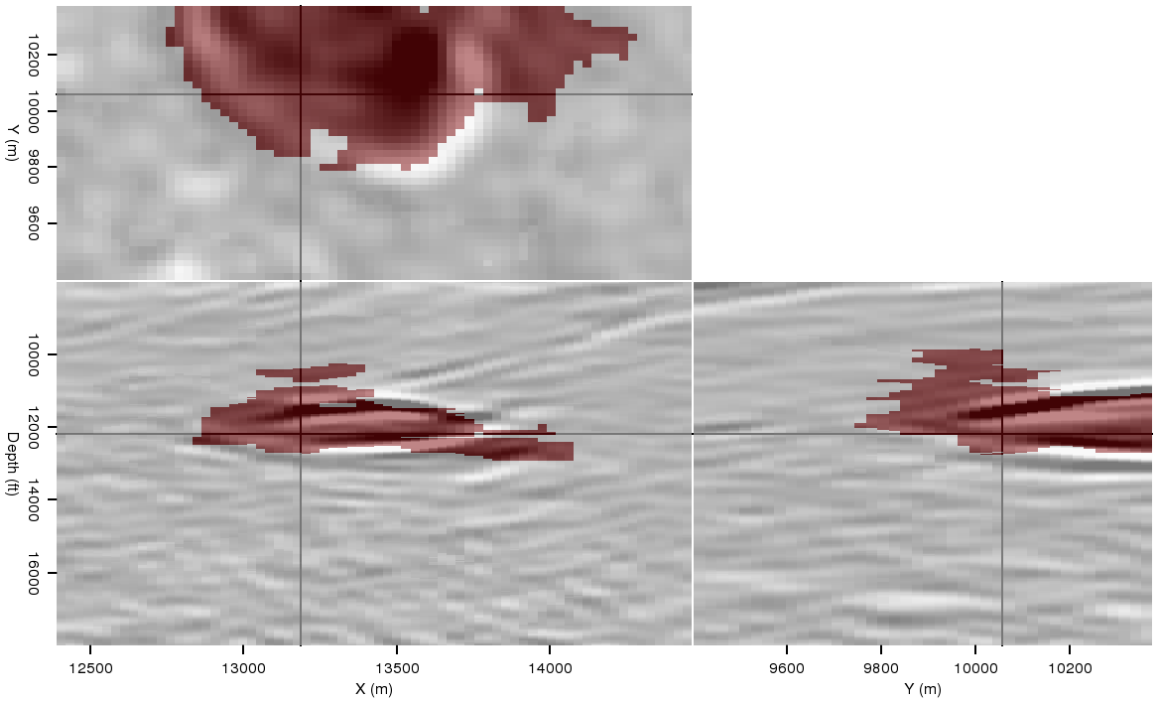

(a)

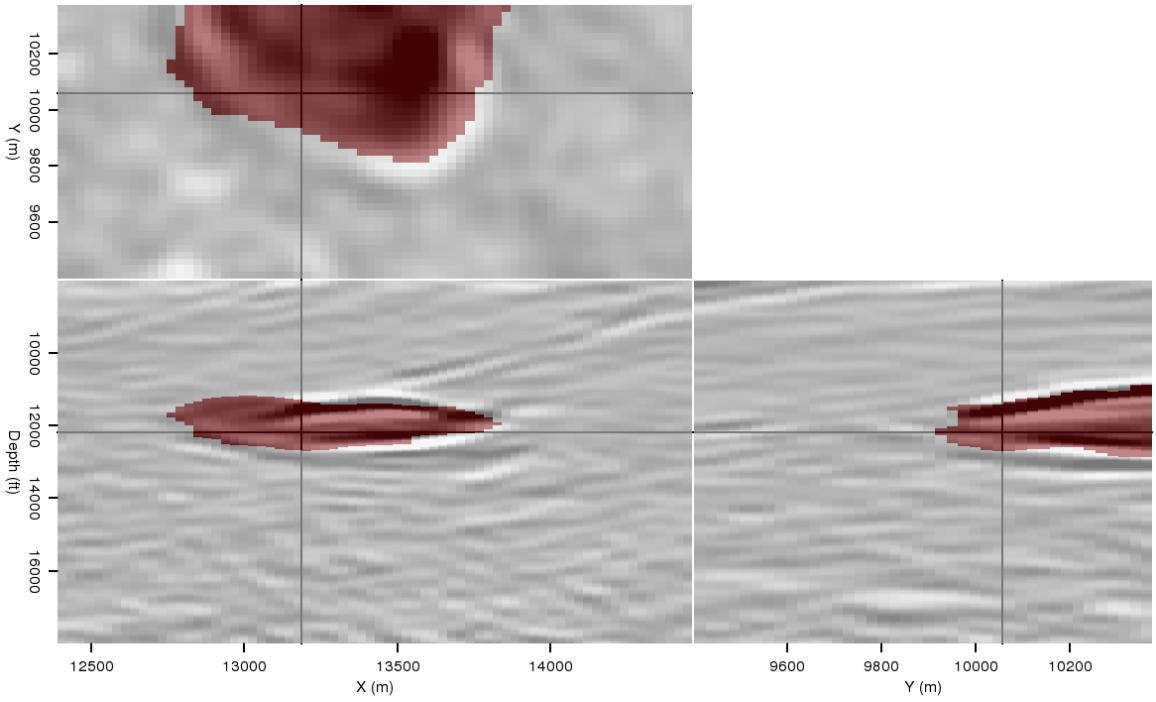

(b)

Figure 12: Automatic segmentation results using (a) the original, unfiltered image and (b) an MH-smoothed image. [**ER**]

Fehmers, G. C. and C. F. W. Hocker, 2003, Fast structural interpretation with structure-oriented filtering: Geophysics, **68**, 1286–1293.

Felzenszwalb, P. F. and D. P. Huttenlocher, 2004, Efficient graph-based image segmentation: International Journal of Computer Vision, **59**, 167–181.

Guitton, A., 2005, Multidimensional seismic noise attenuation: PhD thesis, Stanford University.

Hale, D., 2011, Structure-oriented bilateral filtering of seismic images: SEG Technical Program Expanded Abstracts, **30**, 3596–3600.

Halpert, A., R. G. Clapp, and B. L. Biondi, 2010, Speeding up seismic image segmentation: SEG Technical Program Expanded Abstracts, **29**, 1276–1280.

Tomita, F. and S. Tsuji, 1977, Extraction of multiple regions by smoothing in selected neighbourhoods: IEEE-SMC, **7**, 107–109.

Tukey, J. W., 1971, Exploratory data analysis: Addison-Wesley.

Zahedi, F. and R. Thomas, 1993, A maximum homogeneity based median filter: IEEE Colloquium on morphological and nonlinear image processing techniques, 7/1 – 7/5.